International Journal of Remote Sensing

A land cover distribution composite image from coarse spatial resolution images using an unmixing method

T. M. Uenishi [a]; K. Oki [a]; K. Omasa [a]; M. Tamura [a]

[a] Graduate School of Agricultural and Life Sciences, The University of Tokyo, 1-1-1 Yayoi, Bunkyo-ku, Tokyo 113-8657, Japan

PLEASE SCROLL DOWN FOR ARTICLE

Taylor & Francis
Taylor & Francis Group

A land cover distribution composite image from coarse spatial resolution images using an unmixing method

T. M. UENISHI†, K. OKI*†, K. OMASA† and M. TAMURA‡

†Graduate School of Agricultural and Life Sciences, The University of Tokyo, 1-1-1 Yayoi, Bunkyo-ku, Tokyo 113-8657, Japan
‡National Institute for Environmental Studies Japan, 16-2 Onogawa, Tsukuba, Ibaraki 305-8506, Japan

A method of sub-pixel land cover estimation including an algorithm for minimizing missing data due to cloud cover was proposed for the purpose of evaluating and monitoring the environment of wide areas. A pair of Landsat Thematic Mapper (TM) scenes over coincident multitemporal National Oceanic and Atmospheric Administration (NOAA) Advanced Very High Resolution Radiometer (AVHRR) time-series of directional hemispherical reflectance were used to develop a fine-scale land cover map using either eight or three categories and to estimate the endmembers of the AVHRR image using a positive constrained linear least-squares method. Furthermore, three approaches were evaluated for compositing sub-pixel estimates over cloudy areas in the AVHRR image. Finally, from validation tests made for unmixing and compositing methods, the results suggest that these methods may be generally useful for comparing multispectral images in space and time.

1. Introduction

At present, it has been shown that for environmental assessment, fine spatial resolution images such as Landsat Thematic Mapper (TM) (30 m × 30 m) have been effective in measuring heterogeneous land cover distribution in regions where the objective area is comparatively narrow (Oleson *et al.* 1995). However, when an extensive area such as Asia becomes the object of research, it is difficult to measure the land cover distribution of the entire area with Landsat TM, which can only observe narrow areas. Furthermore, in many areas cloud-free data at fine spatial resolutions are unavailable (Laporte *et al.* 1995). The repeat coverage being every 16 days can also hinder the assessment of vegetation dynamics even in relatively cloud-free areas (Hall *et al.* 1991). This shows that it has been difficult to obtain consistent categories from images taken at different times, due to variability in atmospheric effects, instrumental response, and coarse temporal resolution.

Consequently, the utilization of coarse resolution images, which are useful in monitoring land cover distribution and vegetation transformations at a global scale, can be considered. For example, the Advanced Very High Resolution Radiometer (AVHRR) has been used to produce multitemporal profiles of the Normalized Difference Vegetation Index (NDVI) in order to measure and assess changes in

---

*Corresponding author. Email: agrioki@mail.ecc.u-tokyo.ac.jp

vegetation phenology and conditions (Maselli *et al.* 1998) caused by events such as deforestation. It can also be utilized to perform land-cover type classification at global scales (Tucker *et al.* 1985). Moreover, the frequent repeat cycle of the satellite providing fine temporal data of at least one sample per day depending on latitude, is necessary for monitoring vegetation dynamics. However, its coarse spatial resolution imposes limitations on spectral and spatial information (Cross *et al.* 1991, Malingreau and Belward 1992, Quarmby *et al.* 1992, DeFries *et al.* 1997). In this way, even though coarse resolution satellites can observe the Earth over a short period, many categories are intermingled within each pixel of the observed image. It becomes difficult to determine the categories and to calculate the land coverage with sufficient precision.

To overcome these problems, numerous studies have shown that mixture modelling can be used to estimate vegetation cover (Mackin *et al.* 1990, Smith *et al.* 1990, Roberts *et al.* 1993), and Garcia-Haro *et al.* (1999) have shown that mixture modelling is less sensitive than NDVI to soil background effects. However, in traditional unmixing studies with AVHRR data, it is assumed that only a few endmembers exist throughout an entire image (Robinson *et al.* 2000). For example, Oleson *et al.* (1995) and Oki *et al.* (2002) have retrieved spectral reflectance for each cover type in coarse resolution images using multiple linear regression analysis dealing with only two to four endmembers. In other words, manifold categories have not been dealt with.

Therefore, in this study, a method to calculate the distribution of land cover types around those areas in northeastern Asia within AVHHR mixed pixels was attempted by integrating multitemporal data in a mixture analysis to increase the number of categories that can be analysed.

Moreover, because conventional unmixing studies have not dealt with cloud-covered areas, a method to synthesize a composite image of the unmixed site, for the use of land cover assessment of northeastern Asia was evaluated to eliminate the problem of clouds. To illustrate, Oki *et al.* (2004), have unmixed and validated their results for a wide area; however, only a faveolate map could be produced due to clouds and assessment of the area is difficult. Thus, because atmospheric conditions can hinder the assessment of land coverage, we propose to produce composite images.

Furthermore, a validation test was carried out in order to evaluate the accuracy of the estimated land cover ratio results produced in the composite land cover map. Classified Landsat TM data, which were verified with ground data, were used as the criteria to assess the accuracy of the estimated results.

2. Study site

Because the environment, which is delicate, is easily affected by human development, a method in which the land cover distribution is measured precisely to assess environmental change is necessary. It is impossible to cover expansive areas with tumultuous land cover types in ground data surveys. In order to show that by using remote sensing technology, specific land coverage maps can be synthesized for the use of different environmental research, we have chosen northeastern Asia, shown in figure 1, as a study site to monitor specific land cover distribution due to its vast and diverse land cover types (wetlands, grasslands, evergreen trees, deciduous trees, agricultural areas, urban areas, deserts, rivers, lakes, etc.).
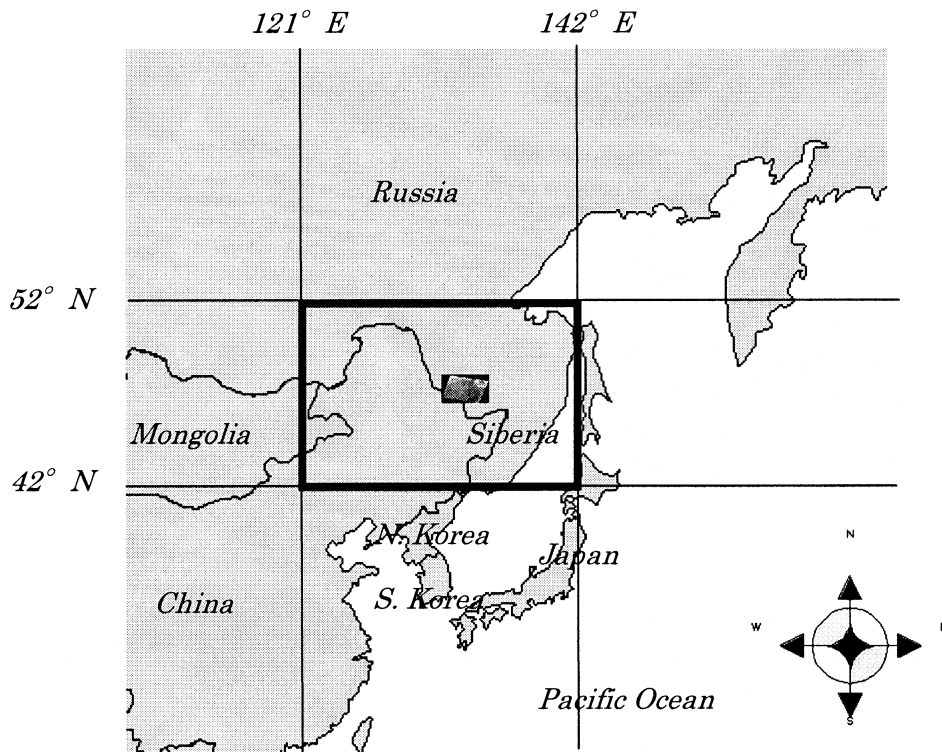
Figure 1. Location of study area in northeastern Asia (upper left coordinate 52° N, 121° E/ lower right coordinate 42° N, 142° E). The image located in the centre is the Landsat TM image (path 116/row 26) used to calculate endmembers and to evaluate results.

In this study, we used Landsat TM (satellite image overlapped onto map in figure 1) and National Oceanic and Atmospheric Administration (NOAA) AVHRR (figure 2) data. We selected this area, because the area within an AVHRR image has the same land cover distribution as a single TM image. Furthermore, the Landsat TM area (path 116/row 26) shown in figure 1 was chosen. This is because a fairly accurate classification map could be produced through verification with land cover data acquired from field surveys on foot and by helicopter using a global positioning system (GPS) digital camera. Landsat TM images (path 116/row 26) from 16 June and 18 July 1997 were selected. Eight NOAA AVHRR images with an upper left coordinate of 52° N, 121° E and lower right coordinate of 42° N, 142° E shown in figure 1, from June–September 1997 were chosen.

3. Algorithm of unmixing method

Generally, when considering coarse resolution images, pixels, which contain multiple categories, can be called mixed pixels. On the other hand, pixels that are made up of a single category are called pure pixels. Spectra of mixtures can be analysed with linear spectral mixture analysis (LSMA), which models each spectrum in a spectral dataset (not necessarily an image) as a linear combination of a finite number of spectrally distinct signatures, referred to as endmembers, with coefficients or fractional abundances between zero and one and summing to one (Adams *et al.* 1986, Smith *et al.* 1990).
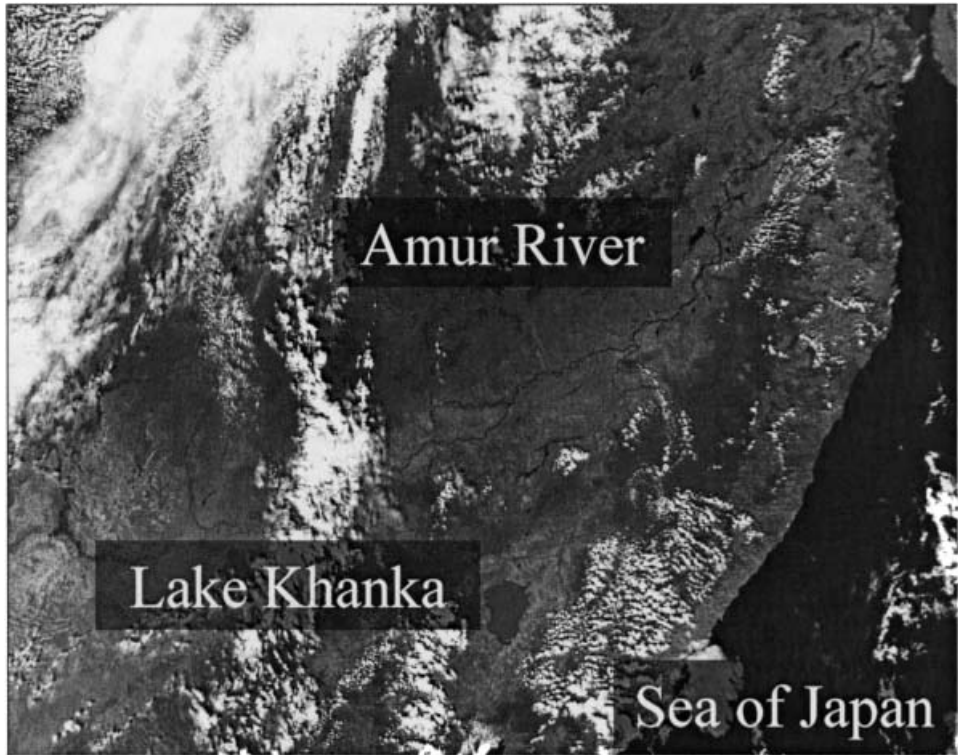
Figure 2. Sample NOAA AVHRR image of a study site projected in Albers Conic Equal Area and resampled at a resolution of 1.1 km using a nearest neighbour interpolation method. (Upper left coordinate 52° N, 121° E/lower right coordinate 42° N, 142° E.)

Endmembers are the features in a scene that are meaningful for an observer, and constitute abstractions of real objects that can be regarded as having uniform properties (Strahler *et al*. 1986). Unless the endmember of a particular category is known, it is difficult to decompose these linear mixture models to calculate the category ratio within a mixed pixel. Because the endmember of each category covered within a pixel must be precisely known before carrying out the unmixing method (Cross *et al*. 1991, Quarmby *et al*. 1992, Foody and Cox 1994), the methods in which these endmembers are determined become vital for LSMA.

It is difficult to identify and estimate the spectral signature of a pure component or endmembers which form the scene, since they vary with the scale and purpose of the study. Several methods have been proposed for estimating the endmembers for each category (Oleson *et al*. 1995, Thompkins *et al*. 1997, Bateson *et al*. 2000, Oki *et al*. 2002). In this research endmembers are estimated by overlapping classified Landsat TM images over AVHRR images and using a positive constrained linear least-squares estimation. Oleson *et al*. (1995) and Oki *et al*. (2002) have also retrieved spectral reflectance for each cover type in coarse resolution images in a similar way using multiple linear regression analysis. However, they only deal with two to four endmembers; in other words, only a few categories can be studied. Moreover, only a limited area is analysed. Therefore, we propose to increase categories and assess a wider range.

First, the total radiance of a coarse resolution mixed pixel can be assumed as a linear sum of the products of the cover type radiance and the cover type weight as a linear spectral mixture. Although pure pixels do not exist in any sort of digital images, we also set the fine spatial resolution pixels as pure such that the cover type radiances are invariant in order to extract details of AVHHR data up to Landsat TM level. Furthermore, for temporal data, we define that the distribution of cover types does not change.

Here, a linear spectral mixture model is a model where the observed radiance of a particular pixel is given as P by endmembers m which include each category with fractional cover ratio a of k types of categories as in the following equation.

$$P = \sum_{j=1}^{k} a_j m_j \tag{1}$$

where,

$$a_j \geq 0 \tag{2}$$

and

$$\sum_{j=1}^{k} a_j = 1 \tag{3}$$

First, the coarse resolution image is geocorrected with the high spatial resolution image as a basis. Next, we assume that a pixel within the high spatial resolution image covers all uniform categories and classify it into k types of categories. By assuming this, we unmix AVHRR images to Landsat TM-level resolution. Here, land coverage a_1 of each pixel in a portion of the coarse resolution image is calculated by overlapping land cover distribution, which is evaluated from a high spatial resolution image, onto the coarse resolution image. Furthermore, the endmember of each category in the coarse resolution image is estimated for each band. If the unknown endmember for the coarse resolution image is m_1, the observed radiance of each pixel within a coarse resolution image p_1 is:

$$p_l = \sum_{j=1}^{k} a_{jl} m_{jl} \tag{4}$$

where

$$m_{jl} \geq 0 \tag{5}$$

In this study, under the constraint of equation (5), we estimated the unknown endmember m_1 of each category in equation (4) using a non-negative least square method.

With the estimated endmembers, the entire coarse resolution image is unmixed using a non-negative least square method for each band. Thus, the land coverage a for each pixel per category throughout the entire coarse resolution image is estimated.

Simple (traditional) unmixing assumes that a set number of endmembers (three or four is a typical number) exists throughout the entire scene, and attempts to find
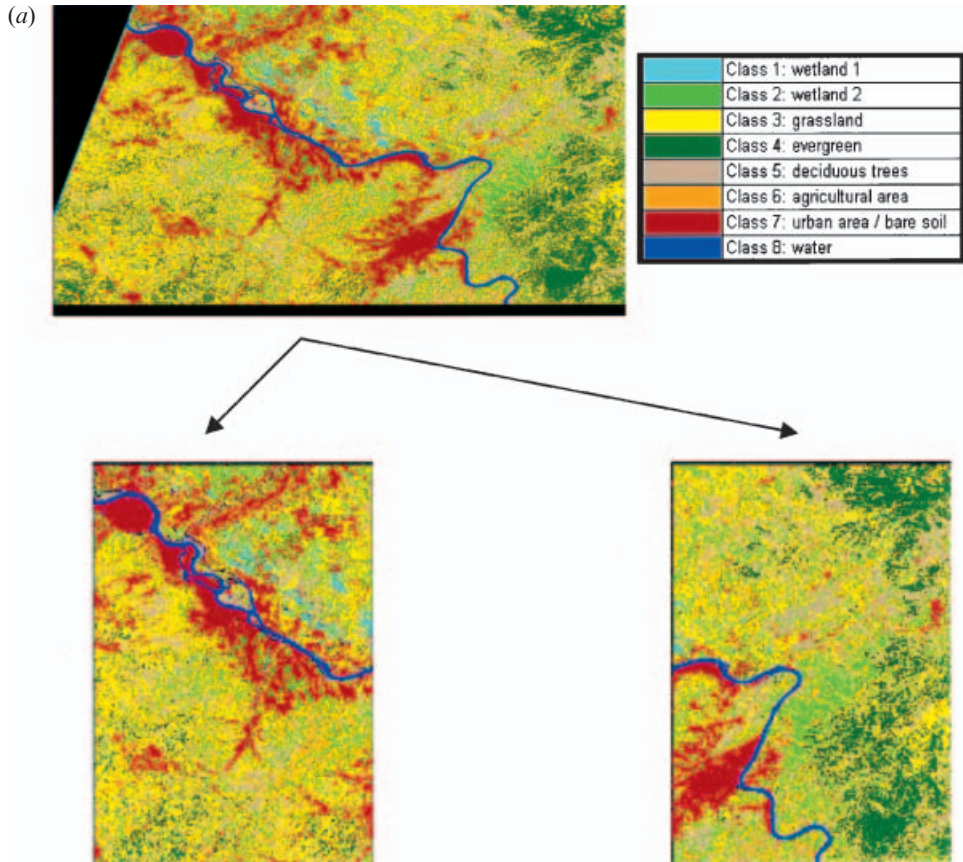
Figure 3.   Fine scale land cover map of a multitemporal Landsat TM image (path 116/row 26). The Landsat TM image was classified into (*a*) eight categories and (*b*) three categories using the ISODATA method and then separated into two images. The bottom left image was used to estimate endmembers. The bottom right image was used for validation purposes.

fractions for these endmembers in every pixel (Robinson *et al.* 2000). In this study, we have applied this unmixing methodology to unmix the AVHRR images into a maximum of eight categories. It was possible to calculate up to eight endmembers by creating multitemporal AVHRR data.

4.   Process and results

4.1   *Atmospheric calibration considerations*

Time-of-flight system and atmospheric calibration data were not available for Landsat or AVHHR images of the study area, nor was it possible to calibrate empirically to ground targets at the time of each overpass of the satellite. A nominal calibration to radiance using preflight instrument calibration data and a standard atmospheric model was not made, because the accuracy of these corrections could not have been verified and any errors in calibration might have propagated undetected into the classification (Sabol *et al.* 1992a, b).
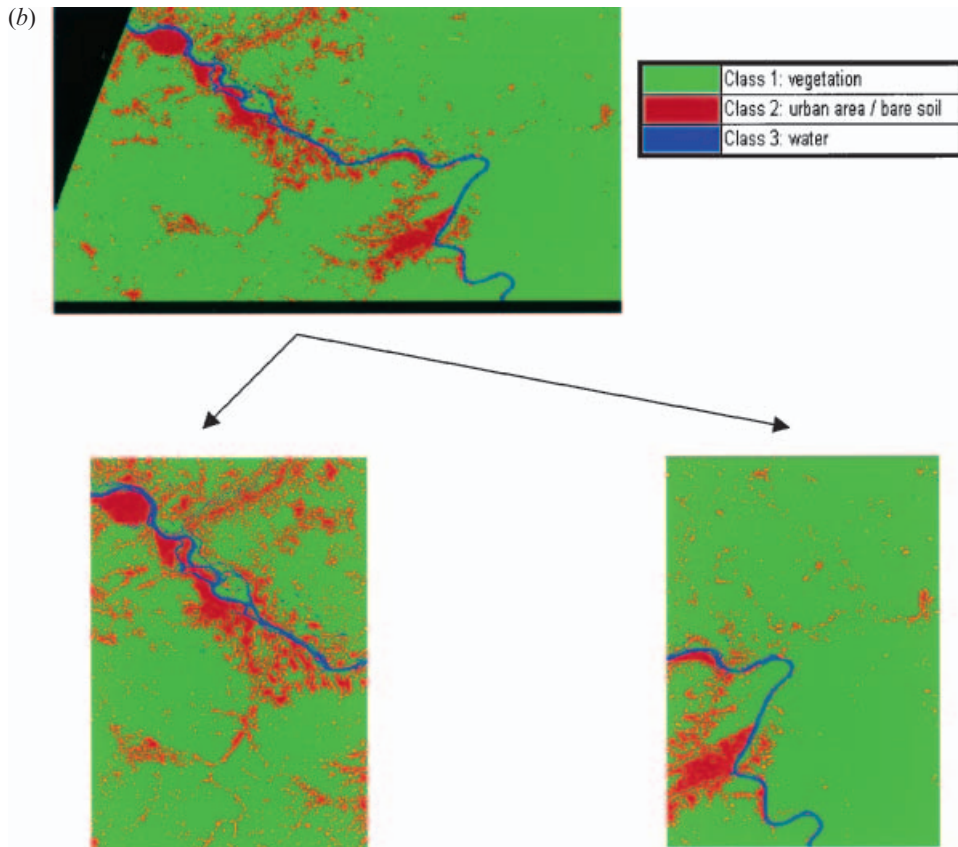
Figure 3.   (*Continued.*)

4.2   *Processing of high spatial resolution image*

In this study, a pair of Landsat TM scenes over the same region is used to develop a fine scale land cover map (eight and three categories) as shown in figure 3(*a*) and (*b*). The Landsat TM image was classified into eight and three categories, using the ISODATA method, assuming that the high spatial resolution image was composed of pure pixels.

Before classifying, the thermal infrared layer (band 6) was removed because of its difference in spatial resolution; thus, a total of six bands using visible and near-infrared images was used. Furthermore, in order to improve the classification accuracy, a multitemporal image dataset was produced from areas with no clouds using two scenes, 16 June and 18 July 1997, producing a dataset with a total of 12 bands. We produced a multidate cloud-free Landsat TM composite dataset in order to investigate various types of land cover that show seasonal characteristics. Thus, depending on the study site, not all sites used in estimating endmembers will need multidate data.

Using an unsupervised classification, the Landsat TM image was ultimately classified into eight categories: wetland 1, wetland 2, grassland, evergreen, deciduous trees, agricultural area, urban area/bare soil, and water (figure 3(*a*)). Furthermore, a three classification (vegetation, urban area/bare soil and water) thematic dataset (figure 3(*b*)) was also created for comparison with the eight category result. Table 1

Table 1. Definitions of nomenclature used in this study.

(*a*) Eight categories

Category number	Category type	Description
1	Wetland 1	Reeds constitute this category; water level is high
2	Wetland 2	Sedges consitute this category; water level is low
3	Grassland	Grasses constitute this category; dry area
4	Evergreen	Evergreens constitute this category; dry area
5	Deciduous trees	Deciduous trees constitute this category; dry area
6	Agricultural area	Areas where agriculture is in activity
7	Urban area/bare soil	Buildings, roads, areas where agriculture is inactive
8	Water	Rivers' lakes, and sea

(*b*) Three categories

Category number	Category type	Description
1	Vegetation	Wetlands, forests, agricultural areas constitute this area
2	Urban area/bare soil	Buildings, roads, areas where agriculture is inactive
3	Water	Rivers' lakes, and sea

shows the definitions for nomenclature of categories used in this study. The classified image was confirmed with ground data produced from field surveys of northeastern Asia.

4.3 *Processing of coarse spatial resolution*

The NOAA AVHHR image was preprocessed by geocorrection at a resolution of 1.1 km. Each NOAA image was corrected geometrically using Landsat TM images as a datum with manual control points. A nearest-neighbour interpolation method was used to prevent the original pixel values from being annulled. As a result, the Root Mean Square Error (RMSE) of the superposed NOAA image was within one pixel.

Next, areas that included clouds in each scene were removed based on a threshold determined for bands 3, 4, and 5 of the AVHHR data. After confirming the removal of cloud pixels common in each image, a multi-temporal image was produced. In this study, full cloud effects are assumed to be composited out. All five bands for each dataset were used; thus, 10 band datasets were produced.

Four multitemporal image datasets, each with a total of 10 bands, were produced combining images from June, July, or September 1997. Four areas that did not have significant amounts of cloud were selected to produce a final composite map. Each dataset was used to compensate another for the unidentified areas. Dataset 1 was a combination of 14 June and 18 July 1997. Dataset 2 was a combination of 16 June and 1 September 1997. Dataset 3 was a combination of 29 June and 5 September 1997. Dataset 4 was a combination of 23 July and 30 September 1997. By producing multitemporal datasets, a more accurate endmember estimation can be calculated.

4.4 *Determining endmembers of coarse resolution images*

After preprocessing each fine and coarse resolution image, endmembers were determined. First, the bottom left image in figure 3(*a*) and (*b*) of the classified

Landsat TM image was overlapped onto each multitemporal NOAA image and the land coverage from each mixed pixel of the overlapped area was calculated. Finally, endmember m_1 in equation (4) was estimated using a least-squares method under non-negative constraints. This method was applied for both eight categories and three categories.

4.5 *Unmixing and validation*

After endmembers were estimated for each land cover type from equation (4) under the constraint of equation (5), they were input into equation (1) and the land cover area of each category was estimated using a least-squares method under the constraints of equations (2) and (3). All four multitemporal AVHRR datasets were each unmixed separately with endmembers determined accordingly. Because the study site consists of the same categories as in the classified map, it was possible to unmix the entire AVHRR data.

Furthermore after unmixing, land cover estimates of each unmixed image were evaluated for accuracy of the unmixing method for both eight categories and three categories. The RMSEs, shown in equation (6), for each category were calculated by comparing estimated results and classified Landsat TM data as a reference of an area that was not used in determining endmembers (bottom right image shown in figure 3(*a*) and (*b*)). Here we defined that the classified Landsat TM image was true.

$$\mathrm{RMSE} = \sqrt{\sum_{i=1}^{n} (\hat{a}_i - a_{ih})^2 \Big/ n} \tag{6}$$

where $\hat{a}$ is each land coverage of a certain category for each pixel estimated by unmixing the AVHRR image; a_h is the true land coverage of the same category for the same pixel in the AVHRR image, calculated by overlapping the land cover distribution that is evaluated from the Landsat TM image on to the AVHRR image; and n is the number of pixels in the validation area of the AVHRR image. Accuracy results of the estimated land coverage for eight and three categories are shown in table 2.

Several conclusions can be drawn about the results from table 2. For eight categories, although the unmixing accuracy was different according to land cover type, it showed that certain categories could be analysed more affectively than others. For example, in this study, the results for wetland 1 and water were estimated with relatively good accuracy. The best RMSE for wetland 1 was 5.2%, and water was 9.6%. Thus, it was shown that if the subject of one's research were about reeds or bodies of water they could be estimated from a coarse resolution image at a relatively good accuracy. On the other hand, categories other than wetland 1 and water, such as deciduous trees, showed poorer results relatively. However, traditionally only approximate land cover types, such as vegetation/soil/water could be distinguished using coarse resolution images. Nevertheless, by using the unmixing method in this study, the analysis of certain land cover types, even deciduous trees, in an extensive area becomes possible. In other words, it is possible to evaluate land cover changes of multiple categories within a pixel with this technique.

The unmixing accuracy was also relatively good for the three category case as shown in table 2, making it possible to evaluate the land cover changes from NOAA images when assessing only three categories.

Table 2. RMSEs of land cover estimates per category of four unmixed AVHRR datasets, (*a*) eight categories and (*b*) three categories.

(*a*) Eight categories

	Dataset 1 RMSE(%)	Dataset 2 RMSE(%)	Dataset 3 RMSE(%)	Dataset 4 RMSE(%)
Wetland 1	5.2	9.3	8.2	9.6
Wetland 2	21.4	19.4	24.1	20.1
Grassland	21.7	27.2	23.8	25.8
Evergreen	32.9	16.0	31.5	34.8
Deciduous trees	34.6	34.1	37.6	39.2
Agricultural area	15.8	36.6	15.5	13.8
Urban area/bare soil	12.1	9.9	6.5	7.4
Water	26.7	9.6	18.0	20.5

(*b*) Three categories

	Dataset 1 RMSE(%)	Dataset 2 RMSE(%)	Dataset 3 RMSE(%)	Dataset 4 RMSE(%)
Vegetation	29.2	13.6	21.9	25.3
Urban area/bare soil	12.1	9.1	5.9	8.4
Water	27.6	11.3	21.2	24.6

4.6 *Compositing method*

The unmixing method used in this study was relatively useful for determining the land cover distribution; however, the presence of clouds prevented the entire site from being evaluated (figure 2). Therefore, a compositing method was proposed to eliminate the issue of clouds and produce a land cover map of a wide area.

When synthesizing a composite image with multiple datasets, areas that overlap geographically become a problem. Theoretically the results for overlapping areas should be the same; however, in reality there is a slight variation in the results. Three approaches were evaluated for compositing the sub-pixel estimates over cloudy areas. The three methods were tested to see which method was optimal in creating a composite image from a number of results. Land cover estimates for each overlapping area were calculated for each category separately.

The first method for determining the pixel value of an overlapping area was to compare RMSE results of the unmixed images. Instead of calculating an RMSE for each category, one RMSE value was calculated for each dataset by using all of the estimated values as one result. The image with the lowest error was selected to represent the overlapping area. Thus, the estimated value for each category was provided by the 'better' image. However, in this case the result depended on the number of pixels in each category.

The second method was to compare the actual estimated results of each category for each overlapping area and simply selecting the better-estimated result for the pixel value of the particular overlapping area in each category.

Finally, rather than comparing, the third method was to calculate the mean of the estimated values of each category for each overlapping area and represent the mean value as the pixel value for each overlapping area in each category.

Furthermore, after producing a composite image for each method, a validation test was made on each composite image to determine the optimal compositing

Table 3. RMSEs of three different compositing methods per category within the composite image for eight categories and three categories.

(*a*) Method 1

Category (8)	RMSE (%)	Category (3)	RMSE(%)
Wetland 1	7.8	Vegetation	16.8
Wetland 2	20.5	Urban/soil	9.1
Grassland	25.7	Water	15.2
Evergreen	20.6		
Deciduous trees	32.5		
Agricultural area	29.2		
Urban/soil	9.4		
Water	12.4		

(*b*) Method 2

Category (8)	RMSE(%)	Category (3)	RMSE(%)
Wetland 1	8.0	Vegetation	14.5
Wetland 2	19.5	Urban/soil	9.5
Grassland	26.0	Water	12.3
Evergreen	17.3		
Deciduous trees	34.3		
Agricultural area	28.2		
Urban/soil	10.1		
Water	10.3		

(*c*) Method 3

Category (8)	RMSE(%)	Category (3)	RMSE(%)
Wetland 1	9.5	Vegetation	14.5
Wetland 2	19.5	Urban/soil	9.2
Grassland	27.3	Water	12.3
Evergreen	17.3		
Deciduous trees	34.3		
Agricultural area	36.0		
Urban/soil	9.9		
Water	10.3		

method. Validation tests were made for each compositing method by calculating the RMSE in equation (6) using an area of the composite image with that of the classified Landsat TM image, which was not used in determining endmembers (bottom right image shown in figure 3(*a*) and (*b*)). Validation results of the estimated land coverage for eight and three categories are shown in table 3.

From validation tests, the optimum method to create an accurate land coverage map was to simply select the best estimation of a given area from unmixed results as shown in method 2 of table 3. By synthesizing composite images, the accuracy of the estimated values was able to be improved. It was possible to improve estimation of land cover area significantly, by comparing both eight and three category accuracy results of single multitemporal datasets, shown in table 2, with the accuracy results from the second compositing method, shown in table 3. This could be explained by the fact that by increasing datasets, estimated values could converge towards the probable value. Therefore, by producing composite images, the environment can be monitored for land cover distribution and vegetation dynamic studies without the
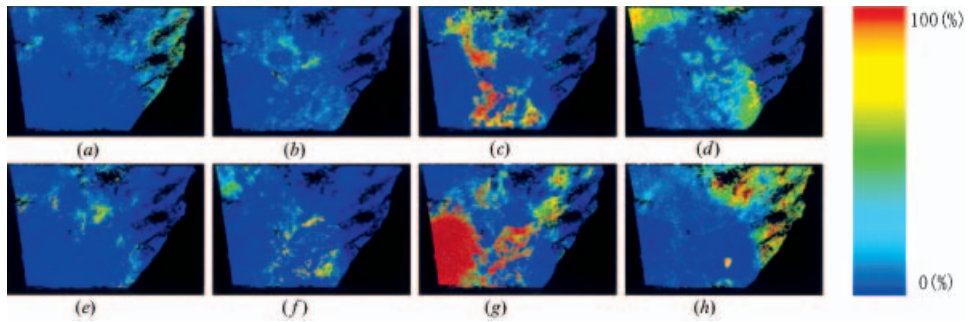
Figure 4.   Composite images of eight categories. The top four categories are (*a*) wetland 1, (*b*) wetland 2, (*c*) grassland, (*d*) evergreen, from left to right. The bottom four categories are (*e*) deciduous trees, (*f*) agricultural land, (*g*) urgan area/bare land (*h*) water from left to right. The colour bar on the right is an index to show the area percentage of a category in a certain pixel. Black regions along the perimeter of the colour image were not used in the calculations (e.g. ocean, distinct land cover distribution), and the black regions within the image could not be embedded with cloud-free data.
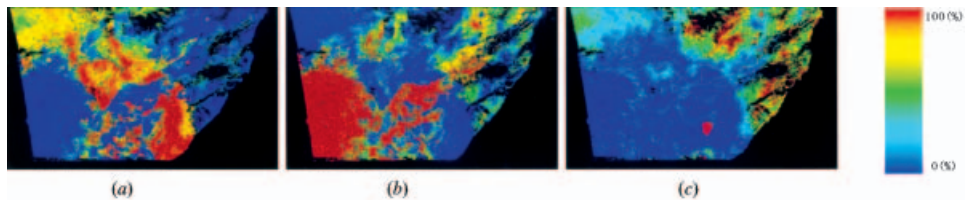
Figure 5.   Composite image of three categories. The categories are (*a*) vegetation, (*b*) urban area/bare land, (*c*) water from left to right. The colour bar on the right is an index to show the area percentage of a category in a certain pixel. Black regions along the perimeter of the colour image were not used in the calculations (e.g. ocean, distinct land cover distribution), and the black regions within the image could not be embedded with cloud-free data.

affects of clouds. The final land distribution composite maps using method 2 for each category are shown in figure 4 and figure 5 for eight categories and three categories respectively. The composite map shows the area ratio of a category within a pixel accordingly with the colour bar. The black regions along the perimeter of the colour image are areas that were not used in the calculations (e.g. ocean, distinct land cover distribution), and the black regions within the image are areas that could not be embedded with cloud-free data.

5.   Discussion

In this way, by increasing datasets and using the proposed composite method, estimated values can be ameliorated while clouds can be totally eliminated at the same time.

Although the error did exceed 30% for some categories as shown in tables 2 and 3, this unmixing and compositing method is considerably useful for quantifying the amount of categories, such as wetland 1. To illustrate, conventionally for NOAA images, the NDVI was calculated to evaluate the quantity of vegetation (Elmore *et al*. 2000). However, only a relative amount of vegetation could be tracked. Because of this fact, it is advantageous that the proposed technique can estimate the quantity of a category.

In order to improve the accuracy of land cover estimates in a wide area for future studies, several points were considered for improvement. To begin with, the spectral signature of the categories in northeastern Asia resembled each other well, so it was difficult to discriminate between them and estimate endmembers. For example, the spectra of deciduous tree and agricultural field resemble each other. McGwire *et al.* (2000) also found that this may occur because two spectral endmembers are so similar, creating non-unique solutions to the mixture equations where noise plays a large factor in pushing the weights to one endmember or the other. Thus, the method can be expected to perform optimally when cover types are spectrally separated and well represented in the area of interest.

Secondly, the accuracy of the classification Landsat TM data, which are assumed to be composed of pure pixels, may not be as high due to current classification methods that are subjective; thus, in the future, a classification method which does not intervene human judgment needs to be developed. Here, the ISODATA method was used to classify the Landsat TM image. This requires human intervention to judge the categories. In this study, a $30\,m \times 30\,m$ spatial resolution surface imagery was used, so it is possible to unmix the NOAA images at a higher accuracy if higher resolution data were used instead.

Moreover, in the future surface radiant exitance-related errors need to be dealt with. Here we assumed that the measured coarse spatial resolution radiance represents the true radiance of the target area. However, errors can be made due to atmospheric attenuation of the signal, solar and viewing geometry (bidirectional effects), subpixel cloud effects, topographical variation, and instrument noise. Thus these problems need to be taken into consideration.

Finally, there was the problem of error caused from the geometric correction of the AVHHR imagery. The conversion RMSE was within one pixel, which equals less than one kilometre difference in the AVHHR imagery. It is difficult to estimate an accurate endmember due to this deviation caused by geometric correction. Currently there are limits to geolocation accuracy for existing fine and coarse spatial resolution satellites due to the fact that the fine and coarse spatial resolution instruments currently orbit different platforms. Puyou-Lascassies *et al.* (1994) also found that the ability to unmix coarse spatial resolution data using fine resolution data is adversely affected by current limitations on coregistration accuracies. However, according to Oleson *et al.* (1995), recently developed techniques for optimally determining spacecraft position and attitude based on high resolution surface maps have demonstrated potential for significantly increasing georegistration accuracies for coarse spatial resolution instruments. In future studies, in addition to taking BRDF effects into account, georegistration techniques may improve the proposed method.

6. Conclusions

A practical method for unmixing mixed pixels of coarse resolution images and synthesizing a land cover area composite image to eliminate the influence of clouds has been proposed. AVHRR radiance measurements were unmixed using co-located Landsat TM land cover for calibration. From this, the land cover area at the subpixel level of a coarse resolution image can be estimated. In this study, the actual land cover distribution within each mixed pixel was measured from AVHRR images of northeastern Asia.

In addition, the verification of the unmixing accuracy was carried out with optimistic results. Over a single scene processed the land cover was estimated with ~20% accuracy for three classes and ~30% accuracy for eight classes. From the RMSE results, it was shown that the land coverage could be estimated at a relatively acceptable accuracy. Although the unmixing accuracy was different according to land cover type, this unmixing method was shown to be effective according to certain objectives, from both results of eight categories and three categories. Moreover, the proposed techniques are a considerable improvement over estimating relative quantity of a category.

Furthermore, a compositing method was considered to be able to evaluate uniform land cover areas to remove the influence of clouds. From validation tests, the best method to create an accurate land coverage map was simply to select the best estimation of a given area from unmixed results. By synthesizing composite images, the accuracy of the estimated values could also be improved. By producing composite images land cover distribution can be monitored without the affects of clouds.

Accumulated data from the past can be used for environmental assessment at a global scale. By using this technique, it is possible to evaluate yearly change of the detailed land cover using coarse resolution images. Furthermore, this study shows that integration techniques that exploit the unique characteristics of multiple instruments are preferable over methods that are compromised by the inherent disadvantages of a single dataset. Thus, by using multiple instruments with the proposed method, the affects of clouds can be removed and information on the status and condition of the existing land types as well as any change occurring in the land type condition over time can be obtained to assess detailed land cover distribution at a global scale for research such as improvement of land management practices on lands susceptible to desertification.

References
ADAMS, J.B., SMITH, M.O. and GILLESPIE, A.R., 1986, Spectral mixture modeling: a new analysis of rock and soil types at the Viking Lander I site. *Journal of Geophysical. Research*, **91**, pp. 8098–8112.
BATESON, C.A., ASNER, G.P. and WESSMAN, C.A., 2000, Endmember bundles: a new approach to incorporating endmember variability into spectral mixture analysis. *IEEE Transactions on Geoscience and Remote Sensing*, **38**, pp. 1083–1094.
CROSS, A.M., SETTLE, J.J., DRAKE, N.A. and PAIVINEN, R.T.M., 1991, Subpixel measurement of tropical forest cover using AVHRR data. *International Journal of Remote Sensing*, **12**, pp. 1119–1129.
DEFRIES, R., HANSEN, M., STEININGER, M., DUBAYAH, R., SOHLBERG, R. and TOWNSHEND, J., 1997, Subpixel forest cover in Central Africa from multisensor, multitemporal data. *Remote Sensing of Environment*, **60**, pp. 228–246.
ELMORE, A.J., MUSTARD, J.F., MANNING, S.J. and LOBELL, D.B., 2000, Quantifying vegetation change in semiarid environments: precision and accuracy of spectral mixture analysis and the Normalized Difference Vegetation Index. *Remote Sensing of Environment*, **73**, pp. 87–102.

FOODY, G. and COX, D., 1994, Sub-pixel land cover composition estimation using a linear mixture model and fuzzy membership functions. *International Journal of Remote Sensing*, **15**, pp. 619–631.

GARCIA-HARO, F.J., GILABERT, M.A. and MELIA, J., 1999, Extraction of endmembers from spectral mixtures. *Remote Sensing of Environment*, **68**, pp. 237–253.

HALL, F.G., SELLERS, P.J., STREVEL, D.E., KANEMASU, E.T., KELLY, R.D., BLAD, B.L., MARKHAM, B.J., WANG, J.R. and HUEMMRICH, H., 1991, Satellite remote sensing of surface energy and mass balance: results from FIFE. *Remote Sensing of Environment*, **35**, pp. 187–199.

LAPORTE, M., JUSTICE, C. and KENDALL, J., 1995, Mapping the dense humid forest of Cameroon and Zaire using AVHRR satellite data. *International Journal of Remote Sensing*, **16**, pp. 1127–1145.

MCGWIRE, K., MINOR, T. and FENSTERMAKER, L., 2000, Hyperspectral mixture modeling for quantifying sparse vegetation cover in arid environments. *Remote Sensing of Environment*, **72**, pp. 360–374.

MACKIN, S., DRAKE, N.A., SETTLE, J.J. and ROTFUSS, J., 1990, Towards automatic mapping of imaging spectrometry data using an expert system and linear mixture model. *Proceedings of the 5th Australasian Remote Sensing Conference, October 1990, Perth, Western Australia*, pp. 8–12.

MALINGREAU, J.P. and BELWARD, A.S., 1992, Scale considerations in vegetation monitoring using AVHRR data. *International Journal of Remote Sensing*, **13**, pp. 2289–2307.

MASELLI, F., GILABERT, M.A. and CONESEC, C., 1998, Integration of high and low resolution NDVI data for monitoring vegetation in Mediterranean environments. *Remote Sensing of Environment*, **63**, pp. 208–218.

OKI, K., OGUMA, H. and SUGITA, M., 2002, Mixel classification of alder trees using temporal Landsat Thematic Mapper imagery. *Photogrammetric Engineering and Remote Sensing*, **68**, pp. 77–82.

OKI, K., UENISH, T.M., OMASA, K. and TAMURA, M., 2004, Accuracy of land cover area estimated from coarse spatial resolution images using an unmixing method. *International Journal of Remote Sensing*, **25**, pp. 1673–1683.

OLESON, K.W., SARLIN, S., GARRISON, J., SMITH, S., PRIVETTE, J.L. and EMERY, W.J., 1995, Unmixing multiple land-cover type reflectances from coarse spatial resolution satellite data. *Remote Sensing of Environment*, **54**, pp. 98–112.

PUYOU-LASCASSIES, P.H., PODAIRE, A. and GAY, M., 1994, Extracting crop radiometric responses from simulated low and high spatial resolution satellite data using a linear mixing model. *International Journal of Remote Sensing*, **15**, pp. 3767–3784.

QUARMBY, N.A., TOWNSHEND, J.R.G., SETTLE, J.J., WHITE, K.H., MILNES, M., HINDLE, T.L. and SILLEOS, N., 1992, Linear mixture modelling applied to AVHRR data for crop area estimation. *International Journal of Remote Sensing*, **13**, pp. 415–425.

ROBERTS, D.A., SMITH, M.O. and ADAMS, J.B., 1993, Green vegetation, nonphotosynthetic vegetation, and soils in AVIRIS data. *Remote Sensing of Environment*, **44**, pp. 255–269.

ROBINSON, G.D., GROSS, H.N. and SCHOTT, J.R., 2000, Evaluation of two applications of spectral mixing models to image fusion. *Remote Sensing of Environment*, **71**, pp. 272–281.

SABOL, D.E., ADAMS, J.B. and SMITH, M.O., 1992a, Quantitative sub-pixel spectral detection of targets in multispectral images. *Journal of Geophysical Research*, **97**, pp. 2659–2672.

SABOL, D.E., ROBERTS, D.A., SMITH, M.O. and ADAMS, J.B., 1992b, Temporal variation in spectral detection thresholds of substrate and vegetation in AVIRIS images. *Proceedings of the Third Annual Airborne Geoscience (AVIRIS) Workshop* (Pasadena, CA: Jet Propulsion Laboratory), pp. 132–134.

SMITH, M.O., USTIN, S.L., ADAMS, J.B. and GILLESPIE, A.R., 1990, Vegetation in deserts I: a regional measure of abundance from multispectral images. *Remote Sensing of Environment*, **31**, pp. 1–26.

STRAHLER, A.H., WOODCOCK, C.E. and SMITH, J.A., 1986, On the nature models in remote sensing. *Remote Sensing of Environment*, **20**, pp. 121–139.

THOMPKINS, S., MUSTARD, J.F., PIETERS, C.M. and FORSYTH, D.W., 1997, Optimization of endmembers for spectral mixture analyis. *Remote Sensing of Environment*, **59**, pp. 472–489.

TUCKER, C.J., TOWNSHEND, J.R.G. and GOFF, T.E., 1985, African land-cover classification using satellite data. *Science*, **227**, pp. 369–375.